1992A&A...263..301M

Astron. Astrophys. 263, 301–311 (1992)

ASTRONOMY AND ASTROPHYSICS

Infrared lines as probes of solar magnetic features

I. A many-line analysis of a network region

K. Muglach[1] **and S. K. Solanki**[2] *

[1] Institut für Astronomie, Universität Graz, Universitätplatz 5, A–8010 Graz, Austria
[2] Institut für Astronomie, ETH–Zentrum, CH–8092 Zürich, Switzerland

Received February 11, accepted May 16, 1992

Abstract. The results of an analysis of Stokes V profiles of all the unblended lines of neutral iron in the infrared H–band (1.5–1.8 μm) are presented. The observational data, obtained in a quiet network region at solar disk center ($\mu = 0.99$) using a Fourier transform spectrometer (Stenflo et al. 1987b), are compatible with an absence of stationary flows larger than ± 0.3 km s^{-1} within the magnetic feature. The infrared Stokes V profiles are asymmetric in the same sense but with less magnitude than the Stokes V profiles of lines in the visible. The influence of the Zeeman effect is investigated using multi-variate regression. It is found that the weak–field approximation breaks down for most H–band lines and that complete splitting is a better approximation for lines with a Landé factor $\gtrsim 1.5$. Finally, numerical radiative transfer calculations are carried out for a sample of 16 Fe I lines to determine further properties of the lower layers of solar magnetic flux tubes. These many–line calculations confirm the results of Zayer et al. (1989) regarding the magnetic structure, derived by them using only 2 lines. An attempt is also made to determine the temperature in the lower (continuum–forming) layers of magnetic elements. The H–band lines are found to be rather temperature insensitive and can constrain the temperature only very roughly. Thus an upper limit of approximately 1.8–2.0 and a lower limit of 0.8 can be set on the continuum contrast of the spatially unresolved magnetic elements relative to the quiet sun.

Key words: solar magnetic fields – magnetic network – flux tubes – infrared spectra – polarimetry

1. Introduction

The promise of the infrared spectrum around 1.5 μm for the study of solar magnetic fields, evident since the pioneering work of Harvey & Hall (1975), cf. Harvey (1977), has remained largely unrealized, with only a handful of publications until now (Stenflo et al. 1987b; Zayer et al. 1989; Livingston 1991; Rabin et al. 1991). In a series of papers initiated by the present one we attempt to fill this gap.

The magnetic field in the solar atmosphere is thought to be concentrated into flux tubes of various sizes. The subject of the present investigation are the magnetic elements which lie at the small–scale end of the size distribution and are so small that they can be spatially resolved only under exceptional circumstances if at all with present instrumentation. The properties of magnetic elements have recently been reviewed by Stenflo (1989), Schüßler (1990) and Solanki (1990).

It is our aim in the present paper to explore the deeper photospheric layers of small–scale magnetic elements. Such information is important for the following reasons:

- MHD waves and oscillations, which heat the chromosphere and possibly the corona, are excited in these layers and the radiation that heats the upper photosphere within the magnetic feature is channelled into the flux tubes at these depths.
- The visible continuum intensity, formed in these layers, is important for the interpretation of observations of magnetic elements. It affects measurements of the magnetic flux and also determines the ionization balance and thus the departures from LTE for many atomic species within magnetic elements. In addition, it influences the global solar luminosity.

The radiation originating deepest in the solar atmosphere is the continuum, particularly the continuum at 1.6 μm (but see Ayres 1990). However, continuum measurements may not be the best instrument to study the properties of the deeper layers of solar magnetic features. Since the non–magnetic surroundings also radiate in the continuum, the exact observed signal depends critically on the spatial resolution of the observations relative to the intrinsic size of the magnetic feature, which may account for the highly divergent results found by Frazier (1971), Worden (1975), Koutchmy (1977), Muller & Keil (1983) and Foukal & Fowler (1984). The correct interpretation of such observations is extremely uncertain due to the often unknown sizes of magnetic features, the unknown properties of their surroundings, selection effects, etc. The interpretation is also complicated by the fact, that many so–called "continuum" or white–light observations include a large contribution from spectral lines formed higher in the atmosphere within the spectral band pass (see e.g. Foukal et al. 1981). Furthermore, the continuum observations do not provide

Send offprint requests to: K. Muglach
*Visiting Astronomer, National Solar Observatory, operated by the Association of Universities for Research in Astronomy, Inc., under contract with the National Science Foundation.

© European Southern Observatory • Provided by the NASA Astrophysics Data System

1992A&A...263..301M

any information on the magnetic field and the velocity within or in the surroundings of magnetic elements.

In the present paper we explore another diagnostic, namely Stokes V profiles of spectral lines in the H–band (1.5–1.8 μm). Due to the minimum of the continuum opacity at 1.6 μm and to the fact that most of the lines have a high excitation potential, we see deeper layers of the photosphere than in the visible. The analysis is carried out in two main steps. Some properties of the lower photospheric layers of the magnetic elements are first derived from a statistical multi–line analysis using all the identified unblended Fe I lines in the infrared H–band. To determine additional physical parameters numerical radiative transfer calculations of a subset of 16 lines are then carried out and compared with the observations.

2. Observational data and line parameters

2.1. Observational data

The spectrum used in this work was acquired on 6th May 1984 with the McMath telescope and the Fourier transform spectrometer (FTS) of the National Solar Observatory at Kitt Peak. A quiet network region very close to solar disk center ($\mu = \cos\theta = 0.99$) was chosen, the Stokes parameters I, V and Q were recorded simultaneously in the wavelength range between 1.5 and 1.8 μm (H–band). Since Stokes Q shows no signal clearly distinguishable from the noise, the analysis concentrates on Stokes I and V. The observations have a spatial resolution of 5″ and a spectral resolving power of 360 000. The effective integration time was 53 min. More details on the data, their acquisation and a description of the reduction procedure has been given by Stenflo et al. (1984, 1987a,b). Individual lines (λ 1.5648 μm and λ 1.5822 μm) of the spectrum used here have been analysed earlier by Stenflo et al. (1987b) and Zayer et al. (1989).

The noise in the spectrum has been determined by calculating the standard deviation from zero of the Stokes V continuum points. The continuum is assumed to cover those wavelengths which have I/I_c values larger than 0.98 (I_c is the continuum intensity). The noise level for Stokes V is found to vary between 3×10^{-4} over most of the spectrum and 6×10^{-4} near the edges of the wavelength range. The noise level in Stokes I is expected to be similar. Our procedure is more reliable for Stokes V and consequently we have not applied it to Stokes I.

2.2. Line parameters

Of the approximately 130 unblended lines in the infrared H–band about 100 have been identified as Fe I lines by virtue of the correspondence between solar and laboratory wavelengths (Solanki et al. 1990). However, of these lines only approximately 60–70 have been identified with a particular transition of the neutral iron atom. To facilitate the analysis of the large number of lines only individual line parameters are investigated. The selected line parameters correspond closely to the ones chosen by Stenflo & Lindegren (1977, for Stokes I) and by Solanki & Stenflo (1984, 1985, for Stokes V), who carried out similar statistical many–line analyses using spectra in the visible.

The following line parameters of Stokes I and V have been determined for all unblended Fe I lines: λ_I, the core wavelength of the I profile, λ_V, the zero–crossing wavelength of Stokes V, λ_b and λ_r, the wavelengths of the maxima of the blue and the red wing of the V profile, the line strength S_I of the intensity profile, defined as the area of the lower half of the line (given in Fraunhofer, i.e. the area in Å times $10^6/\lambda$). We use this parameter instead of the full equivalent width to minimize the influence of small blends in the line wings. Further line parameters are a_b and a_r, the unsigned amplitudes, and A_b and A_r, the unsigned areas of the blue and the red lobes of the V profile, respectively. These parameters may be combined to form the relative area asymmetry δA and the relative amplitude asymmetry δa

$$\delta A = \frac{A_b - A_r}{A_b + A_r},$$

$$\delta a = \frac{a_b - a_r}{a_b + a_r}.$$

The atomic parameters of the spectral lines needed for the statistical analysis are taken from Solanki et al. (1990). The main parameters are χ_e, the excitation potential of the lower level of the transition and $g_{\rm eff}$, the effective Landé factor of the line. Whenever possible we use $g_{\rm eff}$ values which are empirically derived from laboratory experiments, or have been calculated using more realistic atomic physics than LS coupling (e.g. by Kurucz 1991; cf. Mathys 1990).

3. Results of the many-line analysis

In the present section we discuss scatter plots of various measured line parameters as a function of other (observed solar or atomic) line parameters. In the plots which depend directly on purely atomic parameters (i.e. χ_e or $g_{\rm eff}$) only the approximately 60 lines identified in detail are plotted, while in the other figures as many of the unblended Fe I lines are plotted as possible. A few lines have been omitted from all scatter plots. These include very weak lines, i.e. lines with $S_I < 0.5$ F, since they are strongly affected by noise (both the scatter and the error bars of the parameters of those lines become so large that they only clutter up the diagrams, without providing any additional information). We have also omitted the lines listed in Table 2, more details about them are given in Sect. 4.2.

3.1. Velocities

Figure 1a shows the difference between λ_V and λ_I in km s^{-1} as a function of line strength, S_I. The solid line represents a linear regression through the data points, weighted by the inverse of their squared standard deviations. The redshift of the V profiles with respect to Stokes I can clearly be seen. However, as in the visible we have to take into account the blueshift of the Stokes I profiles caused by convective motions of the field–free part of the solar photosphere before interpreting any shifts in physical terms (e.g. Dravins et al. 1981). Nadeau (1988) has carefully analysed the quiet–sun line shifts of Fe I lines in the visible and the infrared H–band. He gives an expression for the granulation–induced shift of the line core $v_{\rm Gran}$ (in km s^{-1}) as a function of line depth and excitation potential [Eq. (1) of Nadeau 1988].

$$v_{\rm Gran} = -0.31 + 0.00134 \cdot (100 \cdot d_I - 37) e^{\chi_e/2.59}, \quad (1)$$

where d_I is the line depth (normalized to the local continuum) of the I profile. The claimed accuracy of this expression is approximately 0.03 km s^{-1}. Using Nadeau's expression we have calculated the granular blueshift for each line which we have then subtracted from the wavelength of the observed Stokes I profile. In Fig. 1b we plot the corrected $\lambda_V - \lambda_I$ vs. S_I. The solid line again represents a weighted linear regression. The number of

© European Southern Observatory • Provided by the NASA Astrophysics Data System

1992A&A...263..301M

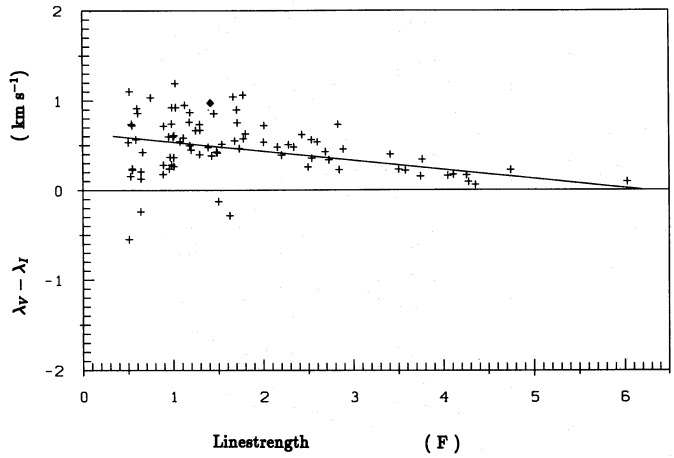

Fig. 1a. The difference between the Stokes V zero–crossing wavelength and the Stokes I core wavelength, $\lambda_V - \lambda_I$, vs. the line strength, S_I. The blueshift of λ_I due to the solar granulation has not been compensated. Each 'plus' symbol represents an unblended Fe I line. The filled diamond represents the $g = 3$ line at 1.5648 μm. Only parameters of lines with $S_I < 0.5$ F have been plotted. A linear, weighted least–squares fit to the data is also plotted

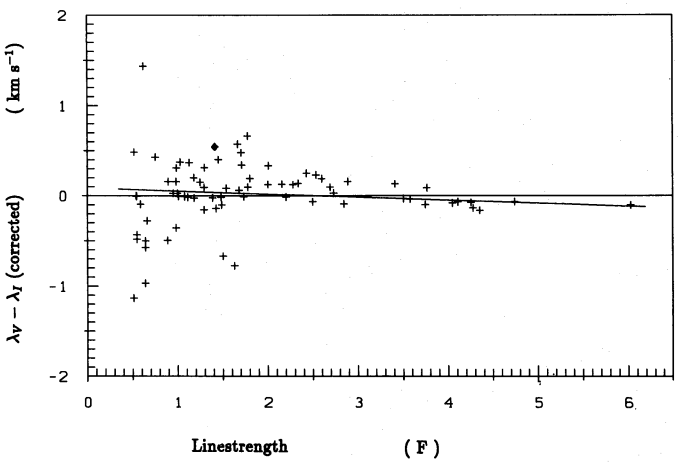

Fig. 1b. $\lambda_V - \lambda_I$ vs. S_I, after compensating for the granulation–induced blueshift of Stokes I according to the formula given by Nadeau (1988), see Eq. (1). Symbols as in Fig. 1a

lines in Fig. 1b is smaller than in Fig. 1a, since χ_e is needed for the correction of λ_I and is unknown for some of the lines in Fig. 1a.

Figure 1b suggests that the deeper layers of flux tubes are free from stationary flows larger than approximately 0.2–0.3 km s^{-1} (0.2 km s^{-1} correponds to the uncertainty of the regression parameters). It may be argued that it is impermissible to subtract quiet–sun granular shifts from the wavelengths of Stokes I profiles measured in the network, but we recall that the estimated magnetic filling factor in the observed region is only 5–7% (Zayer et al. 1989, Sect. 6): Solanki (1986) showed that for regions with such small filling factors the procedure followed here should give results reliable to within the uncertainty quoted above. The present results are in agreement with high spectral resolution observations in the visible (e.g. Stenflo & Harvey 1985; Solanki 1986), but do not agree with previous infrared measurements of Stokes V shifts. Harvey & Hall (1975, see also Harvey 1977) found a Stokes V redshift of 1.6 km s^{-1} compared to Stokes I for the $g = 3$ Fe I 1.5648 μm line (after adjusting for the convective blueshift). Stenflo et al. (1987b) found an adjusted redshift of 0.5–0.6 km s^{-1} for the same line. Since we are analysing the same data set this line shows the same redshift in Fig. 1b (it is marked by a filled diamond). However, since the error bar on $\lambda_V - \lambda_I$ is $\pm$ 0.6 km s^{-1} the zero–crossing wavelength of this line is compatible with an absence of downflows as well. For this line the error is larger than for lines with similar strength but smaller $g_{\rm eff}$, since, due to its large Zeeman splitting, the gradient of V near its zero–crossing wavelength is relatively small. The fact that in order to fit its observed Stokes V profile, the synthetic profiles need not be shifted (see Sect. 5) also supports the conclusion that this line is unshifted.

The Stokes V relative amplitude asymmetry δa is plotted vs. S_I in Fig. 2a, while Fig. 2b shows the relative area asymmetry δA vs. S_I. In both figures a weighted quadratic fit is also plotted.

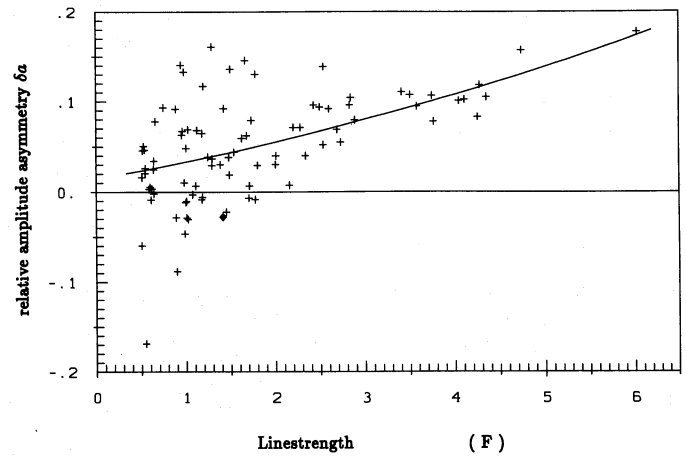

Fig. 2a. The Stokes V relative amplitude asymmetry $\delta a = (a_b - a_r)/(a_b + a_r)$ vs. S_I. a_b and a_r are the unsigned amplitudes of the blue and red lobes of Stokes V, respectively. A quadratic least–squares fit to the data points is also plotted. Symbols as in Fig. 1a

The Stokes V profiles are obviously asymmetric, with stronger blue than red lobes, i.e. δA and δa are positive for lines with $S_I \gtrsim 1.5$ F. For weaker lines the scatter of the data points is too large to make any claims about δa and δA. The sign of the asymmetry and its behaviour as a function of S_I are similar to those of Stokes V profiles in the visible observed near solar disk center. However, the Stokes V asymmetry of H–band lines is smaller than that of lines in the visible by approximately a factor of 1.5–2 (compare with Fig. 12 of Solanki & Stenflo 1984). Since δA is most probably produced by downflows in the surroundings of flux tubes (Grossmann–Doerth et al. 1988; Solanki 1989), this may be caused by a decrease in the granular downflow velocity with depth in the photosphere. On the other hand, the smaller δA near 1.5 μm may simply be due to the much larger Zeeman splitting of the infrared lines, which leads to a reduction of δA according to Grossmann–Doerth et al. (1989a). They showed that δA is largest when $\max(\Delta\lambda_D, \Delta\lambda_H)$ equals the line shift due to the longitudinal velocity gradient. Since for many lines in the H–band $\Delta\lambda_H \gtrsim \Delta\lambda_D$, larger velocities are needed to produce a δA similar to that of lines in the visible (for which $\Delta\lambda_H \lesssim \Delta\lambda_D$). This interpretation is supported by the fact that the $g = 3$ line

© European Southern Observatory • Provided by the NASA Astrophysics Data System

1992A&A...263..301M

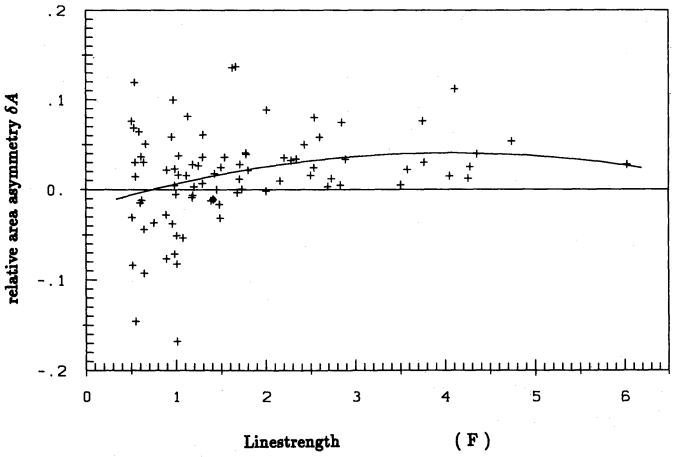

Fig. 2b. The Stokes V relative area asymmetry $\delta A = (A_b - A_r)/(A_b + A_r)$ vs. S_I. A_b and A_r are the unsigned areas of the blue and red Stokes V lobes, respectively. The curve represents a quadratic fit to the data points. Symbols as in Fig. 1a

(λ 1.5648 μm) shows no asymmetry above the noise, although other H–band lines of similar strength and a smaller Zeeman splitting are distinctly asymmetric. Since δa is partly coupled to δA, its reduction presumably has the same source.

3.2. Magnetic field

We investigate the effect of the magnetic field strength on the Stokes V profiles in two ways. Firstly by carrying out multivariate regressions of line parameters that are expected to be affected by the field strength B (e.g. Stenflo & Lindegren 1977; Solanki & Stenflo 1984). Secondly by fitting individual Stokes V profiles (Sect. 5). One reason for trying out regressions in addition to the more exact line–profile fitting is to discover the critical Landé factor above which H–band lines are completely Zeeman split (i.e. $\Delta\lambda_H > \Delta\lambda_D$) in normal flux tubes. Additionally, we want to see whether a regression of H–band lines holds any advantage over regressions of visible lines. This is particularly interesting since regressions (of Stokes I profiles) in the visible have been successfully used to determine cool–star magnetic parameters by Mathys & Solanki (1989).

The result of a regression analysis is illustrated in Fig. 3 for the difference of the wavelengths of the red and the blue Stokes V maxima, $\lambda_r - \lambda_b$. Figure 3a shows the measured $\lambda_r - \lambda_b$ (in km s^{-1}) as a function of normalized Zeeman splitting $g_{\rm eff}\lambda^2$ (in velocity units). Although the data points show a certain scatter, an undeniable trend towards larger peak separation for larger $g_{\rm eff}\lambda^2$ exists. The diamond in the upper right-hand corner is the magnetically very sensitive $g = 3$ line at 1.5648 μm. The field strength can be determined with an accuracy of roughly $\pm$100–150 G from such a diagram. To illustrate this 3 diagonal lines are drawn in Fig. 3. They correspond to the expected splitting, assuming all spectral lines to be completely split, for fields of 1400 G (dotted line), 1550 G (solid line) and 1700 G (dashed line). Note the pivotal role played by the $g = 3$ line. Without it the uncertainty would be considerably larger. According to Zayer et al. (1989) profile fitting to the $g = 3$ line at 1.5648 μm assuming a height–independend field gives 1550 G.

Part of the scatter of $\lambda_r - \lambda_b$ seen in Fig. 3a is due to noise and blends, but some is also due to intrinsically different line widths, different formation heigths, etc. A simple parametrisation of such

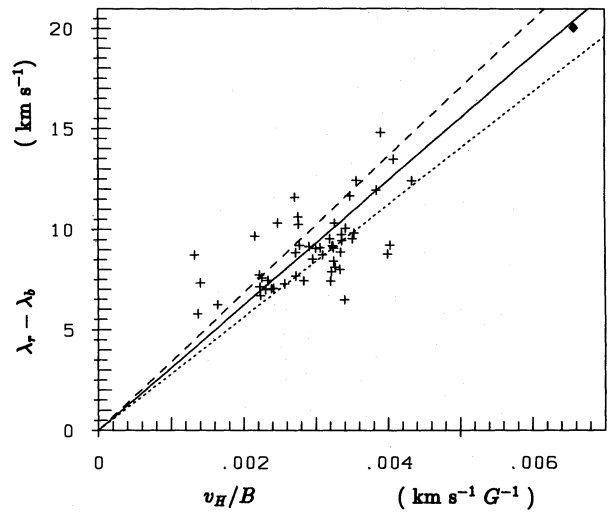

Fig. 3a. Difference between the wavelengths of the red and blue Stokes V maxima, $\lambda_r - \lambda_b$ in km s^{-1}, vs. $v_H/B = 4.67\times10^{-13} g_{\rm eff}\lambda_0 c$, the Zeeman splitting in velocity units for a field strength of 1 G ($g_{\rm eff}$ is the effective Landé factor, λ_0 is the central wavelength and c is the speed of light). The three diagonal lines represent the Zeeman splitting for $B = 1400$ G (dotted line), 1550 G (solid line), and 1700 G (dashed line) under the assumption that all lines are completely split. Symbols as in Fig. 1a

influences in terms of other line parameters was introduced by Stenflo & Lindegren (1977). Following them we use a regression equation that takes into account the influence of line strength S_I, excitation potential χ_e, Zeeman splitting $\Delta\lambda_H/B$ and wavelength λ_0 on $\lambda_r - \lambda_b$:

$$\lambda_r - \lambda_b = x_0 + x_1 S_I + x_2 S_I^2 + x_3\chi_e + x_4\,\Delta\lambda_H/B + x_5\langle g_{\rm eff}\rangle\lambda_0^2. \quad (2)$$

Here $\langle g_{\rm eff}\rangle$ is the average Landé factor of all spectral lines used for calculating the regression coefficients. We find a considerably better fit to the data if we assume the lines to be completely split (i.e. $\lambda_r - \lambda_b \sim \Delta\lambda_H/B = 4.67\times10^{-13} g_{\rm eff}\lambda^2$) than if we use the weak–field–approximation formula of Stenflo & Lindegren (1977) generally applied in the visible (i.e. $\lambda_r - \lambda_b \sim g_{\rm eff}^2\lambda^2/\Delta\lambda_D$), where $\Delta\lambda_D$ is the non-magnetic line width). The exact choice of the wavelength term ($x_5\langle g_{\rm eff}\rangle\lambda_0^2$) is immaterial since all analysed spectral lines have similar wavelengths, so that x_5 is minute.

Figure 3b shows $\lambda_r - \lambda_b$, after subtracting all regression terms except the one describing the Zeeman splitting. The strong influence of the Zeeman splitting on $\lambda_r - \lambda_b$ is now even more evident. Similar plots in the visible show a considerably less clear signature of the Zeeman splitting (Solanki & Stenflo 1984). The magnetic field strength determined from the regression coefficient of the Zeeman term lies around 1440 G if the lines with $g_{\rm eff} \lesssim 1$ are neglected, since for them the approximation of complete splitting is not fulfilled. If all lines are included in the regression, then $B \approx 1200$ G is found.

The H–band is not ideal for determining B using a many–line analysis that does not include radiative transfer, for two reasons: 1. Only about 60 unblended Fe I lines in the whole H–band are sufficiently well identified to be used for such a regression. 2. For a field strength of about 1500 G not all of these lines are completely Zeeman split. Nevertheless, it is still much simpler and more reliable to determine the field strength in a relatively model–independent manner from H–band lines than from lines in the

© European Southern Observatory • Provided by the NASA Astrophysics Data System

1992A&A...263..301M

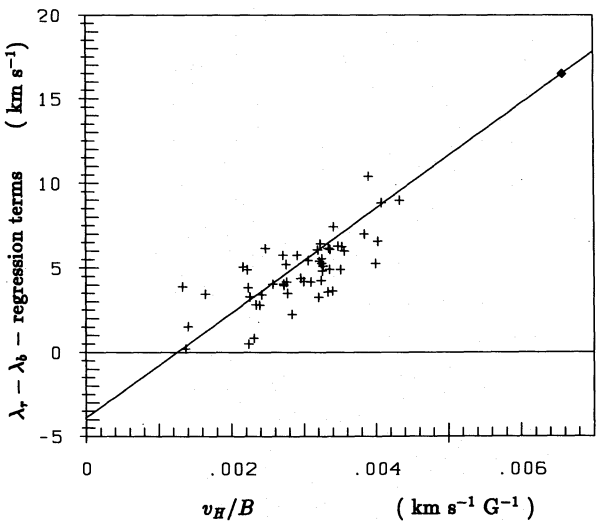

Fig. 3b. $(\lambda_r - \lambda_b - x_0 - x_1 S_I - x_2 S_I^2 - x_3 \chi_e - x_5 \lambda_0^2)c/\lambda_0$, i.e. $\lambda_r - \lambda_b$ after removing non–magnetic dependences with multivariate regression, vs. v_H/B. The slope of the diagonal line corresponds to the splitting induced by $B = 1550$ G. Symbols as in Fig. 1a

visible. We also conclude that when measuring kG field strengths from H–band spectra the multi–variate regression approach gives only unsubstantially better B values than a simple linear fit.

4. Modelling

The second part of the analysis consists of modelling using numerically calculated synthetic Stokes V profiles. We have chosen 16 lines whose Stokes profiles are calculated in various model atmospheres and then compared with the observed ones.

4.1. Model atmospheres

The HSRASP, i.e. the standard HSRA atmosphere (Gingerich et al. 1971), extended to greater depth by attaching it smoothly to Spruit's model of the solar convection zone (Spruit 1974), serves as a model of the quiet sun and of the non–magnetic surroundings of the magnetic elements. Due to the small filling factor of the observed region we expect this to be a relatively good assumption. The main reason we have used the HSRASP instead of a newer model, e.g. Maltby et al. (1986), is that the flux tube models used here were constructed using the HSRASP as reference and, therefore, should only be applied and tested in conjunction with it.

A height–independent microturbulence of 0.8 km s^{-1} is assumed. For the iron abundance we use $\epsilon = 7.56$, and for the empirical fudge factor to the Van der Waals damping constant, calculated using the Unsöld (1955) formula, we use $\delta_\Gamma = 2.5$. This value is recommended for high excitation Fe I lines by Holweger (1979). To reproduce the excess widths of the observed profiles the synthetic lines are broadened with a macroturbulence velocity, whose exact value is determined from a fit to the data.

In order to constrain the flux tube temperature in the deeper photospheric layers, we have used a number of different models to represent the interior of the flux tube. Besides previously existing models (HSRASP, PLA, NET) two families of models in hydrostatic equilibrium have been constructed, starting from the temperature structure of the NET model which is an empirically derived model of the atmosphere within magnetic elements in the solar network (Solanki 1986). The first family of models was constructed by increasing or decreasing the temperature of the NET model in steps of 200 K. The $T(\tau)$ stratifications of the resulting models are all parallel to each other. These models have been named NETP1 – NETP4 in order of increasing temperature. This family of models was only used for test calculations, since NETP1 – NETP4 cannot reproduce line profiles observed in the visible, which are formed higher in the atmosphere. Each of the models belonging to the second family has the same temperature as NET above a certain optical depth at 1.6 μm, $\tau_{1.6}$. Below this optical depth the model may either be hotter than NET (NETH1 – NETH3) or cooler (NETC1 – NETC4). The temperature stratifications of this model family are shown in Fig. 4.

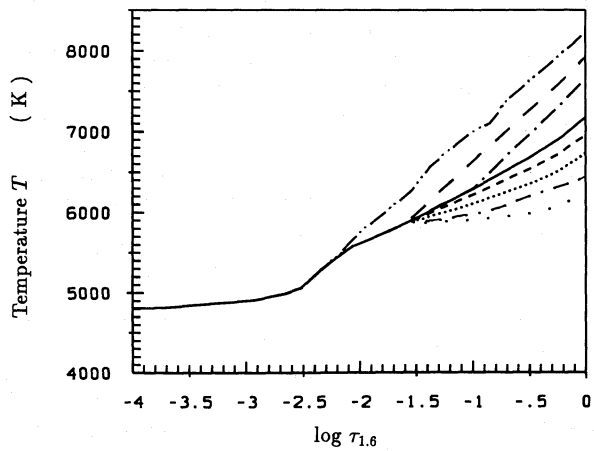

Fig. 4. Temperature T vs. continuum optical depth at 1.6μm, $\tau_{1.6}$, of the models NETH1 (— ·· — ·· —), NETH2 (— — —), NETH3 (— · — · —), NET (——), NETC1 (- - -), NETC2 (· · ·), NETC3 (— — · — — · —) and NETC4 (· · · · ·)

The magnetic field stratifications are calculated by imposing horizonal pressure balance in the thin–tube–approximation. The gas pressure difference between the magnetic and the non–magnetic atmosphere needed to support a field of a given strength is obtained by shifting the internal atmosphere downwards. For the test calculations and the fits we have tried various field strengths between 1900 and 2400 G at $\tau_{1.6} = 1$.

4.2. Selected Lines

From the approximately 60 unblended Fe I lines between 1.5 and 1.8 μm with known atomic parameters we have selected 16 for the radiative transfer calculations. 14 of these lines cover the whole available line strength range and have small Landé factors (between 0.5 and 1.5). The influence of the magnetic field strength on these lines is relatively small but not negligible, so that they serve as diagnostics for the temperature when used in conjunction with a field strength diagnostic [1]. The remaining two lines have $g = 3$ and $g_{\rm eff} = 2$, respectively. They are used to

[1]Due to the a priori unknown filling factor the absolute values of the Stokes V profiles cannot be used for the temperature determination and only ratios between the V profiles of lines with either very different χ_e or different S_I can diagnose the temperature (Solanki & Stenflo 1984, 1985). Since all Fe I lines in the infrared have similar excitation potentials (5.5eV $\lesssim \chi_e \lesssim$ 6.5eV), we concentrate on comparing lines with different S_I values.

© European Southern Observatory • Provided by the NASA Astrophysics Data System

1992A&A...263..301M

constrain the magnetic field strength. In practice we require all 16 line profiles to be reproduced simultaneously. Table 1 lists the 16 selected lines. The first column lists the wavelength of the Stokes I line core in μm, column 2 the transition, column 3 the excitation potential of the lower level of the transition, χ_e, column 4 the effective Landé factor, $g_{\rm eff}$, for which empirically derived values are used whenever possible (Solanki et al. 1990). Column 5 gives the line strength, S_I, determined from the FTS data and column 6 the logarithm of the oscillator strength, log g^*f, determined from a fit to the observed Stokes I profile (see Sect. 4.3).

In the process of line selection we noted a number of Fe I lines whose calculated profiles differed by unrealistically large amounts from the observed ones, particularly in their Zeeman splitting. These lines, together with those which behaved anomalously in the scatter plots, are found in Table 2. Either such lines are misidentified or possibly one of the levels involved in the transitions can not be described by LS coupling. As an example we show in Fig. 5 the fits (dashed) to the observed I and V profiles (solid) of one of these anomalous lines, λ 1.5904 μm.

In Fig. 5a the quite acceptable fit to the Stokes I profile is shown (HSRASP model), while in Fig. 5b the clearly inadequate fit to the Stokes V profile is exhibited. The synthetic Stokes V profile was calculated using the NET model atmosphere and $B = 1500$ G. The $g_{\rm eff}$ value is obviously too large compared to the actual splitting of the line. Since laboratory measurements of g of only the lower level exist (Sugar & Corlis 1985), we have had to use the LS coupling g–value for the upper level. Possibly LS coupling is a very poor approximation for the upper level of this transition. In any case, the identification of this and of the other lines in Table 2 must be reexamined. Thus Fe I 1.5611 μm is most probably also misidentified, in spite of the remark "noise in Stokes V" in Table 2. Any line of its Stokes I strength with $g_{\rm eff} = 1.83$ should posses a sizable Stokes V profile, quite unlike the weak and noisy profile actually observed.

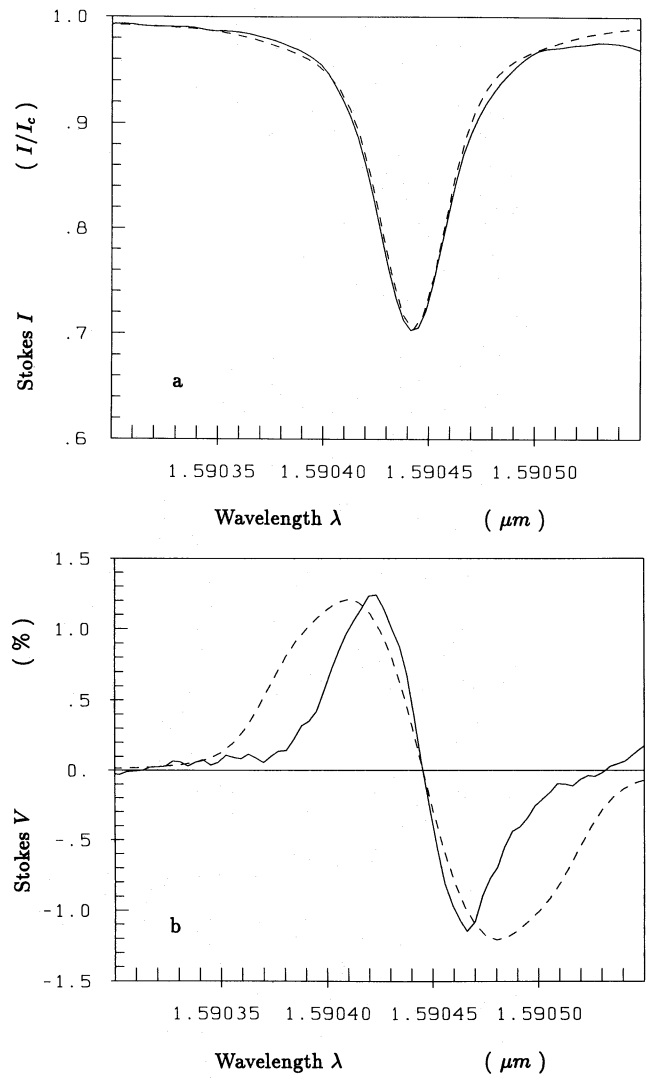

Fig. 5a and b. Observed (solid) and synthetic (dashed) Stokes I and V profile of 1.5904 μm. Stokes I was calculated using an admixture of two model atmospheres, namely 93% of the quiet sun model HSRASP and 7% of NET, while for Stokes V only NET was used

4.3. Initial calculations

The line profile calculations were carried out with the modified Stokes radiative transfer code described by Solanki (1987), which is based on an earlier code written by Beckers (1969a, b).

First the statistically weighted oscillator strengths g^*f of the Fe I lines in Tables 1 and 2 were determined. Profiles calculated using the HSRASP and the NET model atmospheres are weighted (such that the filling factor of NET is 7%) and added together before fitting to the Stokes I profiles observed in the network with log g^*f as a free parameter. Two atmospheric components are required to fit the observed Stokes I profiles, since otherwise systematic differences are found between the calculated V profiles of lines with high and low Landé factor. The resulting log g^*f values are listed in column 6 of Tables 1 and 2. The quality of the fit to Stokes I can be judged from Fig. 6 which shows Stokes I profiles of 4 lines having different S_I and $g_{\rm eff}$ values. The solid profiles are solar, the dashed ones are synthetic. The illustrated quality of the fits is typical for all 16 selected lines.

Next a series of test calculations explores the potential of the selected lines as temperature diagnostics. Both the model families described in Sect. 4.1 are used and the changes in the Stokes V profiles are analysed as the temperature is raised or lowered. Raising the temperature weakens lines having small S_I with respect to lines with larger S_I, while lowering the temperature has the opposite effect. This behaviour is similar to that exhibited by Fe I lines in the visible (Solanki & Stenflo 1984; Keller et al. 1990). However, the magnitude of the effect is considerably lower in the infrared, i.e. the lines are less temperature sensitive, due to their high χ_e values. The ratio between the Stokes V profiles of the strong and weak lines also depends on the gradient of the temperature. A stronger gradient increases the ratio, i.e. mimics a higher temperature. It is not possible, within the bounds of our models, to distinguish between absolute temperature and temperature gradient using infrared Fe I lines alone.

5. Results of the model calculations

For the comparison with the observations we calculate Stokes V profiles in 1.5–D, i.e. the profiles are calculated along a set of vertical rays piercing the model flux tube at different radial distances from its axis. Following Solanki & Roberts (1991) we place the rays such that the points of intersection with the flux tube boundaries are equidistant in height. This scheme is

© European Southern Observatory • Provided by the NASA Astrophysics Data System

1992A&A...263..301M

Table 1. Lines used for radiative transfer calculations.

Wavelength [μm]	Transition	χ_e [eV]	$g_{\rm eff}$	S_I [F]	log g^*f
1.55343	$e\ ^5D_1 - u\ ^5P_2^\circ$	5.64	1.99	1.77	−0.34
1.55667	$e\ ^5G_3 - (3/2)[7/2]_4^\circ$	6.35	1.27	0.55	−0.43
1.56217	$e\ ^5D_4 - t\ ^5D_4^\circ$	5.54	1.49	4.26	0.40
1.56485	$e\ ^7D_1 - 3\ d^6 4s5p\ ^7D_1^\circ$	5.43	3.00	1.41	−0.68
1.57890	$f\ ^5D_4 - (9/2)[9/2]_4^\circ$	6.25	1.47	2.00	0.25
1.58228	$e\ ^5D_1 - u\ ^5F_2^\circ$	5.64	0.74	2.50	−0.10
1.59282	$e\ ^3F_4 - t\ ^3G_4^\circ$	5.95	1.24	0.59	−0.82
1.63163	$e\ ^7G_7 - (9/2)[15/2]_8^\circ$	6.28	1.19	4.28	0.87
1.63245	$e\ ^7D_3 - 3d^6 4s5p\ ^7D_4^\circ$	5.38	1.49	2.16	−0.48
1.64448	$e\ ^5F_5 - 3d^7\ 5p\ ^5F_5^\circ$	5.83	1.41	3.77	0.53
1.64741	$e\ ^3F_3 - t\ ^3G_3^\circ$	6.02	1.01	0.98	−0.42
1.64867	$e\ ^5F_5 - 3d^7 5p\ ^5G_6^\circ$	5.83	1.11	4.35	0.63
1.65245	$f\ ^5F_5 - (7/2)[13/2]_6^\circ$	6.34	0.96	2.84	0.61
1.66614	$e\ ^7F_3 - (7/2)[7/2]_4^\circ$	6.34	0.97	1.43	0.11
1.66931	$f\ ^5F_1 - (1/2)[5/2]_2^\circ$	6.42	0.59	0.64	−0.32
1.70111	$e\ ^3F_4 - 3d^7 5p\ ^3D_3^\circ$	5.95	1.22	1.80	−0.12

Table 2. Lines showing anomalous behaviour.

Wavelength [μm]	Transition	χ_e [eV]	$g_{\rm eff}$	S_I [F]	log g^*f	Remarks
1.56112	$a\ ^1P_1 - z\ ^3P_2^\circ$	3.41	1.83	0.88	–	noise in Stokes V
1.59044	$v\ ^5P_2^\circ - f\ ^3D_1$	5.97	2.36	2.37	0.05	wrong $g_{\rm eff}$?
1.59340	$f\ ^5D_1 - (7/2)[3/2]_2^\circ$	6.31	1.17	0.65	−0.37	wrong $g_{\rm eff}$?
1.59649	$e\ ^5F_3 - 3d^7\ 5p\ ^3G_4^\circ$	5.92	0.77	1.88	−0.09	wrong $g_{\rm eff}$?
1.60518	$e\ ^5G_6 - (9/2)[11/2]_5^\circ$	6.26	1.14	0.28	–	noise in Stokes V
1.61951	$e\ ^7S_3 - (1/2)[7/2]_4^\circ$	6.39	0.70	1.63	0.24	blend in Stokes I
1.66459	$e\ ^5F_2 - 3d^7\ 5p\ ^5D_2^\circ$	5.96	1.25	1.53	−0.25	wrong $g_{\rm eff}$?
1.71611	$f\ ^3F_3 - 3d^7\ 5p\ ^3G_3^\circ$	6.02	0.93	1.45	−0.20	wrong $g_{\rm eff}$?

computationally favourable for the line transfer calculations. The line profiles from all rays are weighted according to the area on the solar disk which they represent and then added together to give a resultant profile which is compared with the spatially unresolved observations.

Since we have no prior knowledge of the filling factor of the observed region, we calculate the profiles along rays out to a fixed radial distance in the 2–D flux tube model. This corresponds to calculating the line profiles for a fixed magnetic filling factor at a given height in the atmosphere. We always ascertain that the flux tube boundary at this radial distance lies well above the formation height of the calculated lines. Since the assumed filling factor in general does not correspond to the true value, the synthetic Stokes V profiles must still be multiplied by a factor F to make them correspond in amplitude to the observed profiles. If the temperature stratification of the model used to calculate the profiles is correct, then the factor F is the same for all lines, if not, then F is a function of line strength and excitation potential. Since the Fe I lines in the H–band all have similar excitation potentials (5.5eV $\lesssim \chi_e \lesssim$ 6.5eV), a plot of F vs. S_I is a diagnostic of the temperature. Another measure of the quality of the fit is the scatter of the F values of the various lines around their means. We qualify this by determining $\chi^2 = \sum_i (F_i - \langle F \rangle)^2 / \langle F \rangle^2$. The smaller the χ^2 the better a given model is. Finally, a successful model must also reproduce the shapes of the V profiles of all 16 lines simultaneously.

Using this approach the models described in Sect. 4.1 are tested against the observed data. However, since they do not reproduce spectral lines in the visible, we have not considered the NETP family of models when comparing with the observations. The temperature stratification of the HSRASP can also be easily excluded. The widths of the V profiles of strong lines calculated in the HSRASP are too large compared to the observations.

For each of the remaining models the high $g_{\rm eff}$ lines are first used to determine the optimum $B(z)$, then the rest of the lines are calculated and used as temperature diagnostics.

In Fig. 7 the F values for the 14 low $g_{\rm eff}$ lines and the 6 atmospheric models are plotted against S_I (triangles: NETH1, crosses: NETH2, open circles: NETH3, open squares: NET, stars: NETC1, plusses: NETC2, filled squares: NETC3, filled circles: NETC4). Linear regressions are also plotted. Both the points and the regressions are shifted vertically for clarity (only the gradient of F vs. S_I contains diagnostic information on the temperature). [2] In order to minimize the influence of the blue–red asymmetry

[2]The F values of the two high $g_{\rm eff}$ lines have been omitted from Fig. 7 and the regression since these two lines are most affected by any small errors in the determination of the magnetic field

© European Southern Observatory • Provided by the NASA Astrophysics Data System

1992A&A...263..301M

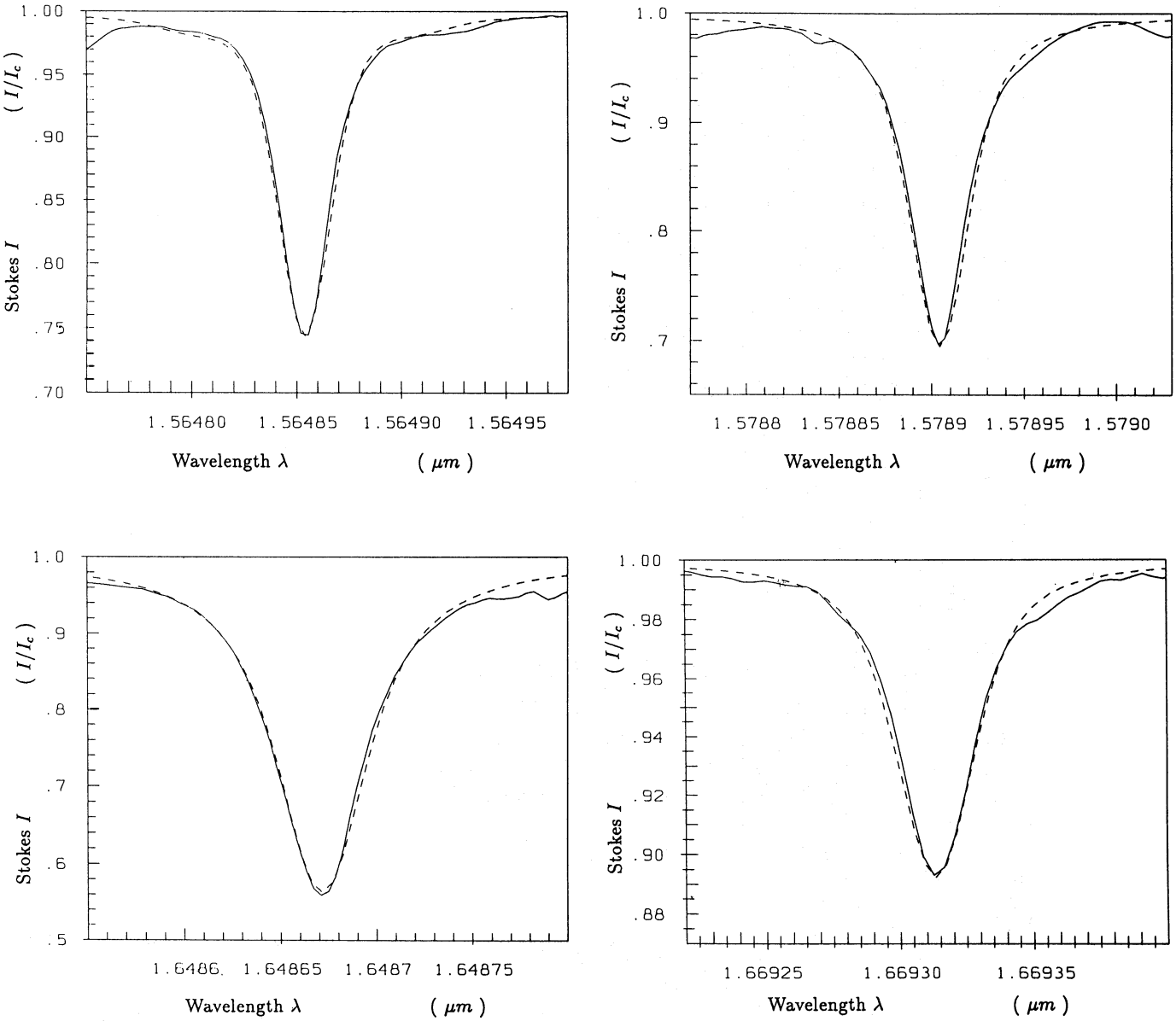

Fig. 6. Stokes I profiles of four Fe I lines: $\lambda 1.5648\mu$m, $\lambda 1.5789\mu$m, $\lambda 1.6486\mu$m, and $\lambda 1.6693\mu$m. The solid curves are the observed profiles, the dashed curves synthetic profiles calculated using the g^*f values in Table 1

of the observed Stokes V profiles (Sect. 3.1) the plotted F values are averaged over both lobes of Stokes V. Fitting the red and the blue lobes separately or symmetrising the observed Stokes V profiles before fitting gives no significantly different results.

Figure 7 illustrates the relative insensitivity of the H–band lines to the temperature in small flux tubes. Consequently we can only set very rough constraints on the temperature in the deeper layers of flux tubes. Although the regression lines of models NETH1 and 2 are distinctly inclined, the eye finds little to distinguish between the gradients of the remaining regressions. In Table 3 we have listed the gradients of the regressions and their standard deviations (column 3), as well as the gradients in units of their standard deviations (column 4), which is a measure of the significance of the gradient. Also listed in Table 3 are the continuum contrast values of the different models (column 2). We define the continuum contrast as $\delta_c = I_c^{magnetic}/I_c^{quiet}$, where I_c is the continuum intensity at 0.5 μm. Finally, in column 5 χ^2, as defined above, is listed.

With the help of Table 3 we can set an upper limit on the temperature in the lower layers of magnetic elements and thus also on δ_c. The gradients of F with respect to S_I suggest that $\delta_c \lesssim 2$ at the 2.5σ level and $\delta_c \lesssim 1.75$ at the 1.5σ level. The total scatter of the F values (χ^2) does not change strongly for $\delta_c \lesssim 1.75$. For larger δ_c values χ^2 increases rapidly. Therefore, we consider $\delta_c \approx 1.75$ an upper limit.

χ^2 increases again for the coolest models (NETC3 and 4) of Fig. 4. In addition, we were unable to reproduce the observed Stokes V profile shapes correctly with NETC4 and cooler models.

strength and would introduce additional uncertainty into the temperature determination. However, it turns out that this is an unnecessary precaution, since these lines fit in very well with the rest.

© European Southern Observatory • Provided by the NASA Astrophysics Data System

1992A&A...263..301M

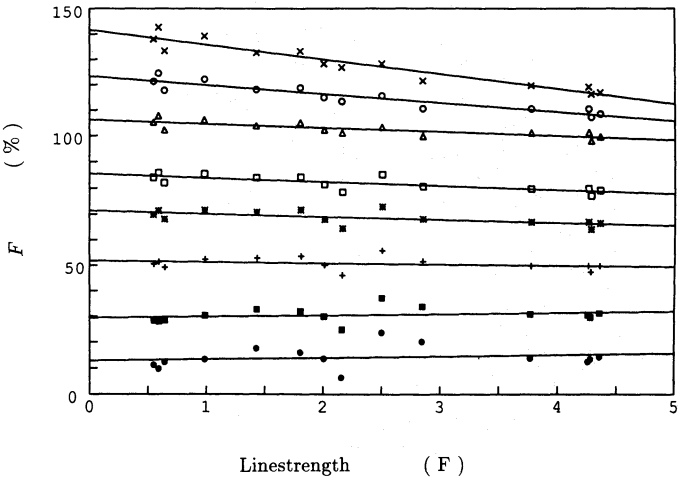

Fig. 7. F vs. S_I resulting from a fit of the synthetic profiles to the observed Stokes V profiles, calculated using, from top to bottom, NETH1 (triangles), NETH2 (crosses), NETH3 (open circles), NET (open squares), NETC1 (stars), NETC2 (plusses), NETC3 (filled squares), NETC4 (filled circles). F is a factor by which the synthetic lines are multiplied in order to fit the observed Stokes V amplitudes. The gradients of the lines fitted through the F values contain diagnostic information on the flux tube temperature

Table 3. Continuum contrast δ_c for $\lambda = 0.5\mu$m, the gradients of the regression lines of Fig. 7 for the various model atmospheres, their standard deviations, their significance and their χ^2–values

Model	δ_c	Gradient	Significance	χ^2
NETH1	2.55	-5.86 ± 1.80	3.3σ	69.85
NETH2	2.01	-3.52 ± 1.41	2.5σ	26.74
NETH3	1.74	-1.58 ± 1.17	1.4σ	7.21
NET	1.38	-1.53 ± 1.31	0.9σ	7.57
NETC1	1.17	-1.17 ± 1.54	0.8σ	6.97
NETC2	1.10	-0.49 ± 1.69	0.3σ	5.75
NETC3	0.99	0.50 ± 2.03	0.2σ	8.10
NETC4	0.81	0.55 ± 2.97	0.2σ	16.92

As with the HSRASP the synthetic Stokes V profiles of the strong lines are broader than the observed profiles, even if the former are unbroadened by any macroturbulence. This allows us to set a lower limit on δ_c, namely $\delta_c > 0.8$.

Finally, Fig. 8 gives 4 representative examples of the 16 selected lines (cf. Fig. 6) as an illustration of the quality of the fit for the model NET which (besides reproducing observations in the visible) gives a slope of F vs. S_I which is compatible with zero. Again, solid curves are observed and dashed ones are synthetic Stokes V profiles. The same mean value of F is used for all the lines plotted in this figure. The fits are acceptable and confirm that this model cannot be ruled out by the present data. Models NETC1 and NETC2 give slightly, but not significantly better fits.

The fact that the shapes *and* amplitudes of the V profiles of both weakly and strongly Zeeman split lines can be reproduced simultaneously suggests that for the observed region the amount of net magnetic flux at $z = 0$ in weak field form ($\lesssim$ 1000 G) is rather small (less than approximately 10% of the total flux). Additional weak flux (i.e. more than is present in the thin–tube–approximation) affects the Stokes V profiles of the strongly split lines mainly near their zero–crossing wavelength, i.e. it does not significantly change the Stokes V amplitudes of these lines. The V profiles of low $g_{\rm eff}$ lines, on the other hand, are affected near their peaks, so that their amplitudes are changed. The presence of significant amounts of a weak field, therefore, changes the ratio of the V profiles of high $g_{\rm eff}$ and low $g_{\rm eff}$ lines, which cannot be reproduced by a single flux tube model, see Ruedi et al. (1992, Paper III of the current series) for more details.

6. Conclusions

We have presented the results of an analysis of an FTS Stokes I and V spectrum in the H–band (1.5–1.8 μm) of a solar network region. A many–line statistical analysis of the measured Stokes V profiles (involving 60–100 spectral lines of neutral iron) leads to the following conclusions:

1. There is no evidence for a systematic up– or downflow greater than 200–300 m s^{-1} within the magnetic elements of the observed region. This is in contrast to results previously published by Harvey & Hall (1975), Harvey (1977) and Stenflo et al. (1987b), who, however, had only considered a single spectral line, Fe I λ 1.56485 μm. We find that the zero–crossing wavelength of this line, due to its large Zeeman splitting, is a very unreliable diagnostic for flows. We claim that for most regions no downflows greater than approximately 250 m s^{-1} are required within small–scale magnetic features at any height between the low chromosphere (Solanki 1986) and the deep photosphere (the present paper) to reproduce spatially averaged observations.
2. The Stokes V profiles in the H–band show a blue–red asymmetry having the same sign as in the visible, but a smaller magnitude. Grossmann–Doerth et al. (1989a) have predicted such a decrease in asymmetry for strongly Zeeman split lines, a condition fulfilled by a large fraction of the H–band lines (see conclusion 3).
3. The lines with $g_{\rm eff} \gtrsim 1.5$ are more or less completely Zeeman split in the observed region and only lines with $g_{\rm eff}$ values well below unity can be considered to be in the weak–field regime. This mixture of lines makes a multi–variate analysis (such as the one developed by Stenflo & Lindegren 1977) difficult for the determination of the field strength. Nevertheless, such an analysis gives, after selecting the most suitable lines, $B = 1450$ G, as compared to 1550 G from line profile fits, and to 1500–1600 G from a linear fit to the Stokes V peak separation of all lines.

An analysis based on radiative transfer calculations of 16 selected spectral lines in a flux tube model gives the following results:

1. A thin tube with a field strength of 2050 G at $\tau_{1.6} = 1$, corresponding to 1500 G at $z = 0$ ($\tau_{0.5} = 1$ of the quiet sun) fits the profiles best. This result is in good agreement with earlier determinations based on H–band (Zayer et al.1989) and visible (Solanki et al. 1987; Zayer et al. 1990) data obtained in the network.
2. An upper limit of 10% can be set on the amount of flux in the observed region which is in weak field form, i.e. with $B(z = 0) \lesssim 1000$ G. This is in good agreement with the results of Zayer et al. (1989) who found that 4 – 7% of the flux is in the form of a 800 G field.
3. Although the 1.5 μm lines are formed deep in the atmosphere, they turn out to be relatively insensitive to temperature.

© European Southern Observatory • Provided by the NASA Astrophysics Data System

1992A&A...263..301M

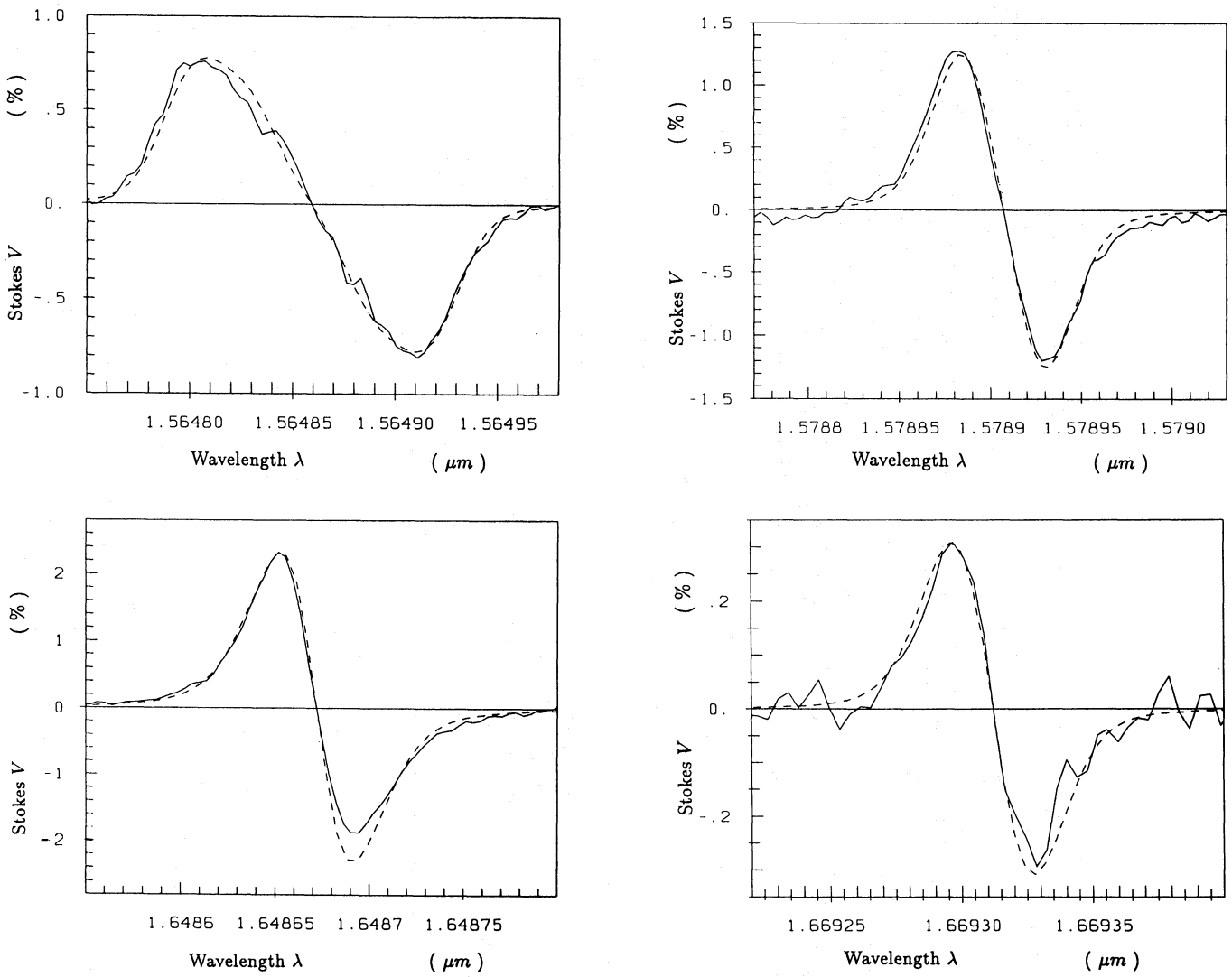

Fig. 8. Observed (solid) and synthetic (dashed) Stokes V profiles of the lines plotted in Fig. 4. The synthetic profiles have been calculated using the NET model. All 4 profiles have been multiplied by the same factor F, i.e. they all correspond to the same filling factor

Therefore, the limits on the continuum intensity in magnetic features $I_c^{magnetic}$ derived here lie relatively far apart. We can set a lower limit of $\delta_c = I_c^{magnetic}/I_c^{quiet} = 0.8$ and an upper limit of $\delta_c = 1.75$–2.0. Data with higher signal-to-noise ratio may permit a better distinction between the various models. Since all measurements of δ_c suggest $\delta_c \lesssim 2$ (e.g. Muller & Keil 1983; Koutchmy 1977; Schüßler & Solanki 1988; Von der Lühe 1989) the present limits do not significantly change our picture of magnetic features. However, the present determination is independent of spatial resolution and gives an average or typical value of δ_c in the network. According to it the $\delta_c \approx 2$ measured by Koutchmy (1977) is very unlikely to be *typical* of small-scale magnetic structures, as has also been argued by Muller & Keil (1983). Consequently, facular models based on this contrast value (Koutchmy & Stellmacher 1978; Stellmacher & Wiehr 1979) are unlikely to describe *typical* magnetic elements. Our limits on δ_c are compatible with δ_c values resulting from theoretical calculations (e.g. Knölker et al. 1988; Grossmann-Doerth et al. 1989b; Steiner & Stenflo 1990).

4. In addition to a microturbulence of 1 km s^{-1} a macroturbulence velocity of 2 km s^{-1} is required to reproduce the Stokes V profiles of all 16 calculated lines. These values are in good agreement with typical turbulent velocities derived in the visible (Solanki 1986; Keller et al. 1990).
5. A filling factor of 5–8% is derived for the region, depending on the model. The best fit models give a filling factor of 6–7% .

Acknowledgements. We wish to thank Prof. H. Haupt for his encouragement and for making this collaboration possible. One of us (S.K.S.) also gratefully acknowledges the hospitality of Prof. Haupt during his stay in Graz.

References

Ayres, T.R.: 1990, in *Solar Photosphere: Structure, Convection and Magnetic Fields*, J.O. Stenflo (Ed.), Kluwer, Dordrecht IAU Symp. **138**, 23

Beckers, J.M.: 1969a, *Solar Physics* **9**, 372

© European Southern Observatory • Provided by the NASA Astrophysics Data System

1992A&A...263..301M

Beckers, J.M.: 1969b, *Solar Physics* **10**, 262

Dravins, D., Lindegren, L., Nordlund, Å.: 1981, *Astron. Astrophys.* **96**, 345

Foukal, P., Duvall, T. Jr., Gillespie, B.: 1981, *Astrophys. J.* **249**, 394

Foukal, P., Fowler, L.: 1984, *Astrophys. J.* **281**, 442

Frazier, E.N.: 1971, *Solar Physics* **21**, 42

Gingerich, O., Noyes, R.W., Kalkofen, W., Cuny,Y.: 1971, *Solar Physics* **18**, 347

Grossmann-Doerth, U., Knölker, M., Schüßler, M., Weißhaar, E.: 1989b, in *Solar and Stellar Granulation*, R.J. Rutten and G. Severino (Eds.), Reidel, Dordrecht, p. 481

Grossmann-Doerth, U., Larsson, B., Solanki, S.K.: 1988, *Astron. Astrophys.* **204**, 266

Grossmann-Doerth, U., Schüßler, M., Solanki, S.K.: 1988, *Astron. Astrophys.* **206**, L37

Grossmann-Doerth, U., Schüßler, M., Solanki, S.K.: 1989a, *Astron. Astrophys.* **221**, 338

Harvey, J.W.: 1977, in *Highlights of Astronomy*, E.A. Müller (Ed.), Vol 4, Part II, p. 223

Harvey, J.W., Hall, D.: 1975, *Bull. Amer. Astron. Soc.* **7**, 459.

Holweger, H.: 1979, in *Proc. 22nd Liège International Astrophys. Symp.*, Inst. d'Astrophysique, Liège, p. 117

Keller, C.U., Solanki, S.K., Steiner, O., Stenflo, J.O.: 1990, *Astron. Astrophys.* **233**, 583

Knölker, M., Schüßler, M., Weißhaar, E.: 1988, *Astron. Astrophys.* **194**, 257

Koutchmy, S.: 1977, *Astron. Astrophys.* **61**, 397

Koutchmy, S., Stellmacher, G.: 1978, *Astron. Astrophys.* **67**, 93

Kurucz, R.L.: 1991, in *Stellar Atmospheres: Beyond Classical Models*, L. Crivellari, I. Hubeny, D.G. Hummer (Eds.) Kluwer, Dordrecht, p. 441

Livingston, W.: 1991, in *Solar Polarimetry*, L. November (Ed.), National Solar Obs., Sunspot, NM, p. 356

Maltby, P., Avrett, E.H., Carlsson, M., Kjeldseth-Moe, O., Kurucz, R.L., Loeser, R.: 1986, *Astrophys. J.* **306**, 284

Mathys, G.: 1990, *Astron. Astrophys.* **236**, 527

Mathys, G., Solanki, S.K.: 1989, *Astron. Astrophys.* **208**, 189

Muller, R., Keil, S.L.: 1983, *Solar Physics* **87**, 243

Nadeau, D.: 1988, *Astrophys. J.* **325**, 480

Rabin, D., Jaksha, D., Plymate, C., Wagner, J., Iwata, K.: 1991, in *Solar Polarimetry*, L. November (Ed.), National Solar Observatory, Sunspot, NM, p. 361

Ruedi, I., Solanki, S.K., Livingston, W., Stenflo, J.O.: 1992, *Astron. Astrophys.* 263, 323 (Paper III)

Schüßler, M.: 1990, in *Solar Photosphere: Structure, Convection and Magnetic Fields*, J.O. Stenflo (Ed.), Kluwer, Dordrecht, IAU Symp. **138**, 161

Schüßler, M., Solanki, S.K.: 1988, *Astron. Astrophys.* **192**, 338

Solanki, S.K.: 1986, *Astron. Astrophys.* **168**, 311

Solanki, S.K.: 1987, *Ph.D.Thesis*, ETH, Zürich

Solanki, S.K.: 1989, *Astron. Astrophys.* **224**, 225

Solanki, S.K.: 1990, in *The Solar Photoshere: Structure, Convection and Magnetic Field*, J.O. Stenflo (Ed.), IAU Symp. *138*, Kluwer, Dordrecht, p. 103

Solanki, S.K.: 1991, in *Cool Stars, Stellar Systems and the Sun VII* J. Bookbinder, M.Giampapa (Eds.), Publ. Astron. Soc. Pacific, Conf. Series, in press

Solanki, S.K., Biémont, E., Mürset, U.: 1990, *Astron. Astrophys. Suppl. Ser.* **83**, 307

Solanki, S.K., Keller, C., Stenflo, J.O.: 1987, *Astron. Astrophys.* **188**, 183

Solanki, S.K., Roberts, B.: 1991, *Mon. Not. Roy. Astron. Soc.* **256,** 13

Solanki, S.K., Stenflo, J.O.: 1984, *Astron. Astrophys.* **140**, 185

Solanki, S.K., Stenflo, J.O.: 1985, *Astron. Astrophys.* **148**, 123

Spruit, H.C.: 1974, *Solar Physics* **34**, 277

Steiner, O., Stenflo, J.O.: 1990, in *Solar Photosphere: Structure, Convection and Magnetic Fields*, J.O. Stenflo (Ed.), Kluwer, Dordrecht IAU Symp. **138**, 181

Stellmacher, G., Wiehr, E.: 1979, *Astron. Astrophys.* **75**, 263

Stenflo, J.O.: 1989, *Astron. Astrophys. Rev.* 1, 3

Stenflo, J.O., Harvey, J.W.: 1985 *Solar Phys.* **95**, 99

Stenflo, J.O., Harvey, J.W., Brault, J.W., Solanki, S.K.: 1984 *Astron. Astrophys.* **131**, 333

Stenflo, J.O., Lindegren, L.: 1977, *Astron. Astrophys.* **59**, 367

Stenflo, J.O., Solanki, S.K., Harvey, J.W.: 1987a, *Astron. Astrophys.* **171**, 305

Stenflo, J.O., Solanki, S.K., Harvey, J.W.: 1987b, *Astron. Astrophys.* **173**, 167

Sugar, J., Corliss, C.: 1985 *J. Phys. Chem. Ref. Data* **14**, Suppl. No. 2

Unsöld, A.: 1955, *Physik der Sternatmosphären*, Springer Verlag, Berlin

Von der Lühe, O.: 1989, in *High Spatial Resolution Solar Observations*, O. Von der Lühe (Ed.), National Solar Observatory, Sunspot, NM, p. 147

Worden, S.P.: 1975, *Solar Physics* **45**, 521

Zayer, I., Solanki, S.K., Stenflo, J.O.: 1989, *Astron. Astrophys.* **211**, 463

Zayer, I., Solanki, S.K., Stenflo, J.O., Keller, C.U.: 1990, *Astron. Astrophys.* **239**, 356

This article was processed by the author using Springer-Verlag LaTeX A&A style file 1990.

© European Southern Observatory • Provided by the NASA Astrophysics Data System